energies

MDPI

Article

Predictive Control Applied to a Solar Desalination Plant Connected to a Greenhouse with Daily Variation of Irrigation Water Demand

Lidia Roca [1,*], Jorge A. Sánchez [2,†], Francisco Rodríguez [2,†], Javier Bonilla [1,†], Alberto de la Calle [3,†] and Manuel Berenguel [2,†]

1 Centro Mixto CIESOL, CIEMAT-Plataforma Solar de Almería, ctra. de Senés km. 4,5 Tabernas 04200, Almería 04120, Spain; javier.bonilla@psa.es
2 Centro Mixto CIESOL, Universidad de Almería, ceiA3, Universidad de Almería, ctra. Sacramento s/n, Almería 04120, Spain; jorgesanchez@ual.es (J.A.S.); frrodrig@ual.es (F.R.); beren@ual.es (M.B.)
3 CSIRO Energy Technology, 10 Murray Dwyer Ct, Mayfield West, Newcastle, NSW 2304, Australia; alberto.calle@psa.es
* Correspondence: lidia.roca@psa.es; Tel.: +34-950-387-800 (ext. 964); Fax: +34-950-365-015
† These authors contributed equally to this work.

Academic Editor: Filippo Sgroi
Received: 23 January 2016; Accepted: 26 February 2016; Published: 14 March 2016

Abstract: The water deficit in the Mediterranean area is a known matter severely affecting agriculture. One way to avoid the aquifers' exploitation is to supply water to crops by using thermal desalination processes. Moreover, in order to guarantee long-term sustainability, the required thermal energy for the desalination process can be provided by solar energy. This paper shows simulations for a case study in which a solar multi-effect distillation plant produces water for irrigation purposes. Detailed models of the involved systems are the base of a predictive controller to operate the desalination plant and fulfil the water demanded by the crops.

Keywords: process control; modelling; solar energy; dynamic simulation; multi-effect distillation

1. Introduction

Modern agricultural systems are characterized by the intensive and optimal use of land and water, turning agricultural exploitation into a semi-industrial concept. Greenhouses are systems suitable both for zones with unfavourable climatic conditions, allowing crop growth regardless of the ambient temperature, and for regions with less restrictive weather, with the aim in this case of increasing crop productivity and improving fruit quality. The greenhouse environment is ideal for farming, because there are variables that can be manipulated to achieve optimal growth and plant development. Control of greenhouse crop growth requires energy consumption, depending on the crop's physiological requirements and, additionally, depending on the production patterns adopted for yield quantity and timing. This crop growth control is achieved through adequate manipulation of climatic variables of the environment and the amount of water and fertilizers applied through irrigation.

Productivity optimization through efficient and adequate irrigation is a basic objective in those countries with water limitations. This resource scarcity is increasing due to the recent rapid expansion of the surface area occupied by greenhouses in the Mediterranean Basin. Consequently, this has also led water to become an important actor in the sustainability of the greenhouse-based system in southeastern Spain.

This water consumption has been progressively depleting the aquifers in the area [1]. Eighty percent of the irrigation water used in Almería (Spain) comes from underground sources, leading to

localized over exploitation of aquifers [2]. Over the last few years, as in other arid and semi-arid areas of the world, the use of alternative water sources has been promoted, such as purified water, rain and condensed water collection as a secondary source, the reuse of drainage water, the development of new technologies related to water-use efficiency, such as advanced irrigation controllers, and sea water desalination.

In this line, the idea of integrating solar desalination systems in the agricultural environment has been significantly considered with the aim of dealing with water limitations in some regions of the planet. One of the most simple and inexpensive techniques, solar stills [3], can be easily combined with greenhouses [4]. Nevertheless, as explained in [4], water produced by a solar still is not enough for growing a crop. This paper deals with the combination of a greenhouse and solar multi-effect distillation (MED) unit. It consists of taking advantage of the water produced in the MED unit to feed a greenhouse, both systems being located in the southeast of Spain. The challenge is to properly operate the desalination plant to produce the daily water demanded by the crop.

Most of the optimization algorithms applied to desalination processes deal with the design of cogeneration plants [5–8]. The objective function includes thermodynamic and environmental issues. However, few optimization problems are focused on satisfying a variable water demand. In the present paper, a two-layer controller that combines basic controllers with model predictive control (MPC) is applied to find and follow proper temperature setpoints in the MED unit and in the solar field. The idea is to analyse if it is possible to maintain a desired volume of distillate obtained by means of a solar desalination process despite the variable consumed water by irrigation in the greenhouse.

2. Case Study

The case study explored in this paper is a micro-grid framework in which two interconnected plants must be managed; a greenhouse and a solar desalination plant (see Figure 1). On the one hand, the greenhouse demands fresh water daily for irrigation purposes, and on the other hand, a solar desalination plant produces distillate water in a multi-effect distillation unit. An intermediate storage tank is assumed to be located between the production process and the consumer system. An explanation of the facilities involved is included in the following sections.

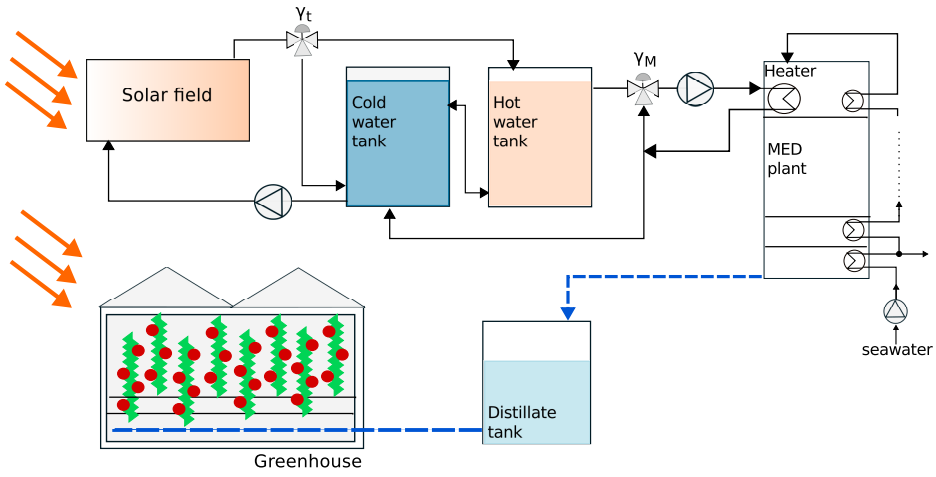

Figure 1. Solar desalination plant coupled with a greenhouse.

2.1. Solar Desalination Facility

The desalination plant used in this study is the AQUASOL system [9] (see Figure 2) situated at Plataforma Solar de Almería (PSA), a dependency of the Centro de Investigaciones Energéticas, Medioambientales y Tecnológicas (CIEMAT) in the south of Spain. This pilot plant includes a

forward-feed vertically-stacked MED unit with 14 cells coupled with a solar collector field (although the system was designed to operate also with fossil energy, this work only deals with the solar operation mode). As shown in Figure 1, seawater is pumped and preheated towards the first cell evaporator (or heater) of the MED. There, water is sprayed on the external surface of the horizontal tube bundle, and part of the seawater is evaporated by the release of the sensible heat of the hot water. A small part of the steam generated in this evaporator preheats the seawater, whereas the main part reaches the evaporator of the next stage, providing the required thermal power to continue the partial evaporation of the feedwater. Similar condensation/evaporation processes are repeated from the second to the 14th evaporators. The steam generated in the last effect is condensed in the final condenser (cooled by seawater). A more detailed description of the MED unit can be found in [10].

The required hot water for the heater is provided by the solar field that supplies hot water to the storage system (two 12-m^3 water storage tanks). A three-way regulation valve, γ_M, is used to reach the nominal temperature at the inlet of the heater, by mixing water from the hot tank with that returned from the heater.

When the solar field temperature exceeds the one in the hot tank, the on-off valve position, γ_t, is changed to connect these components. Otherwise, the solar field should be connected to the bottom part of the cold water tank to avoid cooling down the hot water tank.

Figure 2. Solar desalination facility at PSA-CIEMAT. From left to right and from top to bottom: cold and hot tanks, MED unit and solar field.

2.2. Greenhouse Environment

The research greenhouse used in this work (see Figure 3) is located at the Experimental Station of Cajamar Foundation (El Ejido) in the province of Almería in SE Spain (2°43'W, 36°48'N, and 151-m elevation). The crops were grown in two multi-tunnel greenhouses. Each greenhouse has an area of 800 m^2, with a crop area of 616 m^2 with polyethylene cover; each has automated ventilation with lateral windows in the northern and southern walls, a flap roof window in each span and mesh-protected anti-trip bio-nets, 20 × 10 in thickness. The orientation of the greenhouses is E-W; with crop rows aligned N-S. Cropping conditions and crop management were very similar to those in commercial greenhouses.

A meteorological station is available outside the greenhouses, where air temperature and relative humidity, solar and photosynthetic active radiation, rain detection, wind direction and velocity measurements are taken. During the experiments, some indoor climate variables were also measured:

air temperature, relative humidity, solar radiation, photosynthetic active radiation (PAR), CO_2 monitoring, soil temperature at 3 cm and 40 cm, leaf and substrate temperature, leaf wetness, as well as electrical conductivity and pH monitoring in irrigation and drainage water. All sensors were located in the centre of the greenhouse; the psychrometer and CO_2 sensor at a height of 2.5 m are just above the mature crop; and the PAR and solar radiation sensors at a height of 3.5 m. Table 1 shows the different sensors installed in the greenhouse, its model and brand, range and accuracy.

Table 1. Different variables sampled with the main characteristics of the sensors installed.

Variable	Manufacturer	Model	Range	Accuracy
Air temperature	Vaisala	HMP60	−40 – 0 °C	0.5 – 0.6 °C
Air relative humidity	Vaisala	HMP60	0% – 100%	3% – 5%
Solar radiation	Delta Ohm	LP PYRA 02	0 – 2000 W/m^2	10 $\mu V/(W/m^2)$
PAR radiation	Kipp & Zonnen	Par Lite	0 – 1300 W/m^2	0.2% /°C
Rain detection	Vaisala	DRD11A	Yes/no	—
Wind velocity	Young	12102	0 – 60 m/s	0.5 m/s
Wind direction	Campbell SCI	W200P-1	360°	2°
CO_2 concentration	Vaisala	GMP220	0 – 2000 ppm	2%
Soil temperature	Decagon Devices	RT-1	–40 – 80 °C	0.5 °C
Leaf temperature	PhyTech	LT-2M	5 – 50 °C	0.5 °C
Substrate temperature	Decagon Devices	RT-1	–40 – 80 °C	0.5 °C
Leaf wetness	Decagon Devices	LWS	Yes/No	—
pH	Hannah Instruments	HI 98143	0 – 14	2%
EC	Hannah Instruments	HI 98143	0 – 5000 microS/cm	2%

The crop grows in coconut coir bags with six plants and three droppers each. The irrigation is automated by a demand tray, which is formed by two crop bags. Drainage water is set at a 20% volume. All of the actuators are driven by relays designed for this task. All data are recorded every 30 s with a personal computer.

Figure 3. Greenhouse facilities used for the experiments performed in this work. From left to right and from top to bottom: greenhouse, dropper, solar and PAR radiation device at the outside, irrigation system, solar and PAR radiation device inside the greenhouse and the tomato crop lines.

3. Dynamic Model of the Case Study

The proposed case study is used to simulate a control system, which manages the solar desalination plant operation to fulfil the water demanded by the crops. Therefore, it has been necessary to develop a model able to represent the behaviour of both processes properly. A description of the variables and subscripts involved are included in Nomenclature

3.1. Greenhouse Model

In general terms, without taking into account the specific subsystems for each greenhouse, the air temperature $T_{a,int}$ can be modelled using the following balance [11]:

$$c_{p,a}\rho_a \frac{V_g}{A_{ss}} \frac{dT_{a,int}}{dt} = Q_{cnv,cv-a} + Q_{cnv,ss-a} - Q_{ven} - Q_{trp,cr} \quad (1)$$

where $Q_{cnv,cv-a}$ is the convective flux with the cover, $Q_{cnv,ss-a}$ is the convective flux with the soil surface, Q_{ven} is the heat lost by natural ventilation and the heat lost by infiltration losses, $Q_{trp,cr}$ is the latent heat effect from crop transpiration and $(c_{p,a}\rho_a V_g)/A_{ss}$ is the product of specific air heat, the air density and the effective height of the greenhouse defined as the greenhouse volume and soil surface area.

3.1.1. The convective flux with the cover ($Q_{cnv,cv-a}$).

The convective heat transfer per unit area from the inside air to the cover is calculated based on the difference between the cover temperature, T_{cv}, and the greenhouse air temperature, $T_{a,int}$ [11]:

$$Q_{cnv,cv-a} = f(h_{cnv,cv-a}, T_{cv}, T_{a,int}, V_{cv}, A_{ss}) \quad (2)$$

where V_{cv} is the cover volume and $h_{cnv,cv-a}$ is the cover's inside convective heat transfer coefficient based on the difference between the cover temperature and the internal air temperature and the mean greenhouse air speed. In order to simplify the model, the approach proposed in [12] has been used: if the internal air temperature is higher than the cover temperature, the heat transfer is turbulent; otherwise, the heat flux is laminar.

3.1.2. The convective flux with the soil surface ($Q_{cnv,ss-a}$).

The convective heat transfer per unit area from inside air to soil surface, T_{ss}, is calculated in the same way as the cover convective fluxes using the following equation [11]:

$$Q_{cnv,ss-a} = f(h_{cnv,ss-a}, T_{ss}, T_{a,int}) \quad (3)$$

where $h_{cnv,ss-a}$ is the inside soil surface convective heat transfer coefficient based on the difference between the soil surface temperature and the internal air temperature and the mean greenhouse air speed over the soil surface. Using the studies in [13], the conductive flux between the soil surface and the first soil layer is calculated based on the assumption that the heat flux is one-dimensional (Z axis).

3.1.3. The heat lost by natural ventilation and infiltration (Q_{ven}).

The heat lost per unit area by the natural ventilation term is modelled according to the American Society of Agricultural Engineers (ASAE) Standard Heating, Ventilating, and Cooling Greenhouses (EP406.3) [14] as a function of volumetric flow rate, q_{ven}, greenhouse temperature and external air temperature ($T_{a,ext}$) [15]:

$$Q_{ven} = f(q_{ven}, T_{a,exh}, T_{a,int}, T_{a,ext}, \rho_a, c_{p,a}, A_{ss}) \quad (4)$$

where q_{ven} is described in Equation (5) and $T_{a,exh}$ is the exhaust air temperature, calculated as a linear combination of external and internal air temperatures [16]. This term includes the heat lost

by infiltration losses, as shown in the volumetric flow rate equation, which is based on the thermal buoyancy and wind forces and is described as:

$$q_{ven} = f(q_{loss}, l_{ven,cord}, T_{a,int}, T_{a,ext}, v_{w,ext}, n_{ven}, l_{ven}, d_{ven}, g, k_w) \quad (5)$$

where q_{loss} is the leakage when the vent is closed, n_{ven} is the number of vents, l_{ven} is the length of the vents, d_{ven} is the discharge coefficient, g is the gravity constant, k_w is the wind-effect coefficient, $l_{ven,cord}$ is the cord joining the two extremities of the vent based on the position of the vent, U_{ven}, using the following equation:

$$l_{ven,cord} = f(U_{ven}, w_{ven}) \quad (6)$$

where w_{ven} is the width of the vent.

The leakage when the vent is closed, q_{loss}, is based on the external wind speed ($v_{w,ext}$):

$$q_{loss} = f(v_{w,ext}, v_{w,ext,lim}) \quad (7)$$

where $v_{w,ext,lim}$ is the wind speed, considered as the limit between high and low wind speeds.

3.1.4. The latent heat effect of the crop transpiration ($Q_{trp,cr}$).

The crop itself affects the greenhouse air temperature. As no leaf area measurements are available, it is not possible to use a convective factor in the heat balance equation functioning as a boundary variable. One way to model the effect of the crop on the air temperature is based on the latent heat caused by plant transpiration, described by the following equation [17]:

$$Q_{trp,cr} = \lambda \dot{M}_{trp,cr} \quad (8)$$

where $\dot{M}_{trp,cr}$ is the crop transpiration and λ is the latent heat of evaporation. Most transpiration estimators are based on the Penman–Monteith equation [17,18]. This equation essentially combines the heat transfer equation between the crop and the surrounding air mass. A simplified pseudophysical transpiration model can be used, based on two main variables: the solar radiation arriving at a particular depth in the plant canopy and the vapour pressure deficit [17]:

$$\dot{M}_{trp,cr} = f(I_{crop}, DPV, LAI, k_l) \quad (9)$$

where k_l is the light extinction coefficient for the crop (this is related to the leaf inclination angle and the leaf arrangement with regard to the Leaf Area Index, LAI, and provides an indication of the plant's efficiency at intercepting solar radiation), DPV is the vapour pressure deficit and I_{crop} is the global radiation reaching the crop.

The model of absolute humidity, $H_{a,int}$ (water vapour content of the greenhouse air), is based on a water vapour mass balance equation. The vapour outflow takes place through condensation on the internal side of the cover, crop transpiration, ventilation and vapour lost by infiltration losses. As artificial water influxes (cooling, fogging, *etc.*) are not installed in the greenhouses in which the experiments were carried out, $H_{a,int}$ is modelled using the water mass balance equation given by Equation (10). Based on the mass flux processes, the greenhouse air humidity can be modelled using the equation developed in [11]:

$$\rho_a \frac{V_a}{A_{ss}} \frac{dH_{a,int}}{dt} = \dot{M}_{trp,cr} + \dot{M}_{evp,ss} - \dot{M}_{cd,cv} - \dot{M}_{ven,int-ext} - \dot{M}_{loss} \quad (10)$$

where $\dot{M}_{trp,cr}$ is the crop transpiration flux described in Equation (9), $\dot{M}_{evp,ss}$ is the soil surface evaporation, $\dot{M}_{cd,cv}$ is the condensation flux from the cover, $\dot{M}_{ven,int-ext}$ is the outflow by natural ventilation, $\dot{M}_{loss}$ are the humidity losses by infiltration, and it can be obtained from Equation (7). $\dot{M}_{ven,int-ext}$ is described by the following equation [11]:

$$\dot{M}_{ven,int-ext} = f(q_{ven}, H_{a,int}, H_{a,ext}) \tag{11}$$

where $H_{a,ext}$ is the external air absolute humidity, and the volumetric flow rate, q_{ven}, is described in Equation (5).

3.2. Solar Desalination Plant Model

The model of the solar desalination plant is divided into three main components; the solar field, the storage system and the MED unit. Figure 4 shows a diagram with the connections between these models.

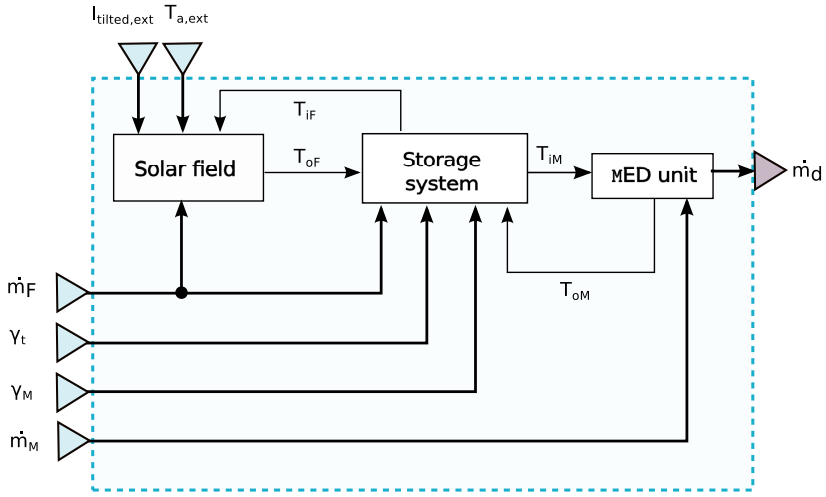

Figure 4. Connection between the submodels of the solar desalination plant.

Solar field outlet temperature, T_{oF}, is obtained with a lumped-parameter model based on an energy balance [19], and the storage tanks have been characterized with energy and mass balances [20]. For the MED unit, the dynamic model developed in Modelica [21] and validated with data from the PSA facility has been used as the reference. With the aim of reducing the computational effort, this model has been simulated to obtain two first-order models that give the distillate mass flow rate, $\dot{m}_d$, and the outlet MED temperature, T_{oM}, as a function of the inlet MED temperature, T_{iM}, assuming nominal conditions in the heater flow rate, $\dot{m}_M$=12 L/s, seawater temperature of 22.3 °C, 4.4 kg/s as the condenser mass flow rate and 2.2 kg/s as the seawater mass flow rate:

$$\dot{m}_d(s) = \frac{0.0137}{5s+1} T_{iM}(s) \tag{12}$$

$$T_{oM}(s) = \frac{0.94}{8s+1} T_{iM}(s) \tag{13}$$

To obtain the above models, the step response method has been applied [22]; the input variable, T_{iM}, was changed with different amplitudes, and the output signals, $\dot{m}_d$ and T_{oM} were recorded to identify the relation between the input and the outputs. The dynamic responses have been represented with the Laplace transform, because its algebraic form is simple [23]; the transfer functions are useful to extract systems information; and it is easy to include them in the simulation tool (MATLAB).

A comparison between the results obtained with both models is shown in Figure 5.

3.3. Global Irradiance

The study presented in this paper combines two facilities (the greenhouse and the solar distillate plant), which are located in two different research centres and whose irradiance measurements cannot

be compared. Since the greenhouse model requires more meteorological variables as inputs, the solar desalination model uses solar irradiance measurements from the greenhouse as input. Nevertheless, this irradiance is measured on a horizontal surface, and it has been transformed to solar irradiance on a tilted surface [24] to take into account the solar field inclination (36°).

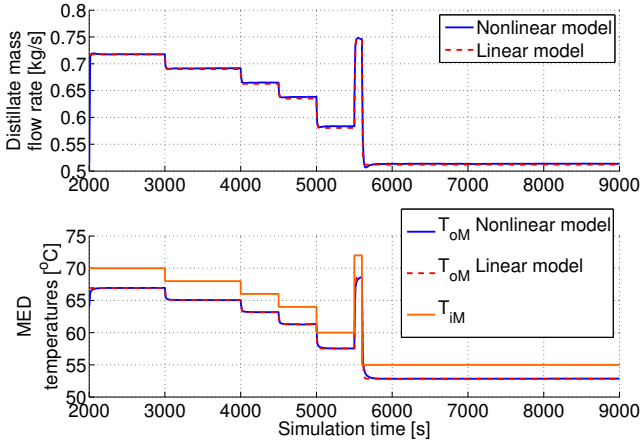

Figure 5. Results obtained with the MED unit first-order model.

4. Control Scheme

The idea behind the controller proposed in this section is to maintain a desired volume of distillate, $V_{d,ref}$, taking into account the variable quantity of water demanded by the greenhouse. The proposed scheme (see Figure 6) includes a state machine, a reference layer and a regulatory layer. The models presented in Section 3 are used to estimate the future water consumption and desalination system temperatures that are used by the reference layer to evaluate optimal setpoints for the temperatures at the inlet of the MED heater and at the outlet of the solar field. These two variables can be regulated, in the regulatory layer, by means of the valve γ_t and water mass flow rate, $\dot{m}_F$, respectively. Both layers are activated when the MED unit is running (CM=1), where CM is defined by the state machine on the basis of the rules explicitly imposed (see Section 4.1).

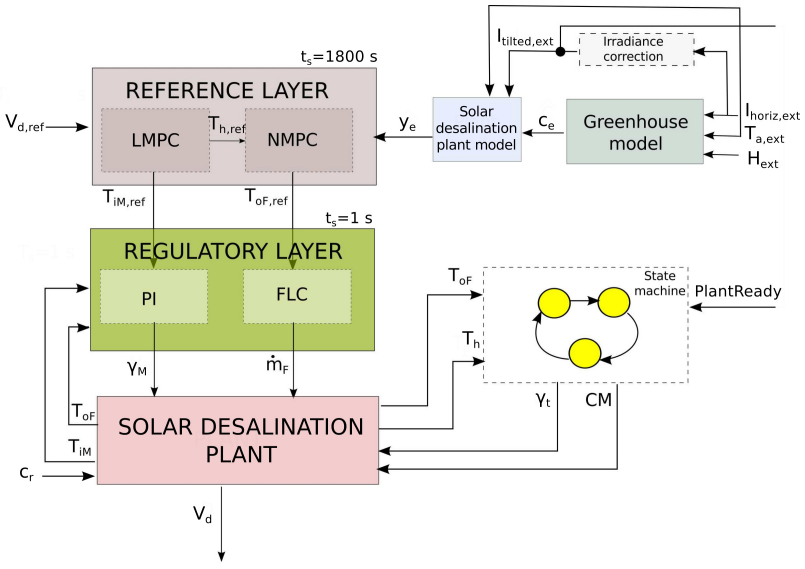

Figure 6. Proposed control scheme to obtain a desired volume of distillate

4.1. State Machine

The state machine chooses one of these four operating modes:

- MED in solar mode: the MED unit is running, and the heated water by the solar field flows to the hot tank. CM = 1, γ_t = 0.
- MED in solar recirculation mode: the MED unit is running, and the valve γ_t is switched, so that the tanks and the solar field are decoupled. CM = 1, γ_t = 1. This mode is used to avoid cooling situations in the storage system due to a downfall in the solar field temperature.
- Solar-field mode: the MED unit is stopped because the temperature is not high enough in the hot tank, and the heated water by the solar field flows to the hot tank. CM = 0, γ_t = 0.
- Solar-field recirculation mode: the MED unit is stopped, and the solar field water recirculates to increase its temperature. CM = 0, γ_t = 1.

The inputs required by this state machine are the signal *PlantReady*, temperature in the hot tank, T_h, and temperature at the outlet of the solar field, T_{oF}.

This state machine includes the following conditions:

- *PlantReady* AND ($T_h \geq$66 °C) $\longmapsto$ CM=1 (MED running),
- NOT(*PlantReady*) OR ($T_h \leq$50 °C) $\longmapsto$ CM=0 (MED stopped),
- (T_{oF}-T_h) $\geq$3 °C$\longmapsto$ γ_t=1 (solar field to hot tank),
- (T_{oF}-T_h) $\leq$1 °C$\longmapsto$ γ_t=0 (solar field recirculation),

where *PlantReady* is a manual input provided by the plant operator who must take into account the irradiance conditions and check that the vacuum system (to remove the air and the non-condensable gases generated during the desalination process) is ready at the MED unit.

4.2. Reference Layer

To reach the desired volume of distillate water, two previous steps are recommended: to calculate the required MED inlet temperature and to choose the appropriate solar field temperature setpoint with the aim of reaching a high enough temperature in the hot tank.

As described in Section 3.2, the distillate production and MED inlet temperature are linearly dependent, so a linear model predictive controller (LMPC) can be used to calculate the setpoint, $T_{iM,ref}$, taking into account the temperature constraints: there is a maximum temperature, to avoid scale formation in the heater, 72 °C, and a minimum temperature is also defined to assure a minimum distillate production: 55 °C $\leq T_{iM,ref} \leq$ 72 °C.

On the other hand, a nonlinear model predictive controller (NMPC) is used to solve an optimization problem, to calculate a reference for the outlet solar-field temperature and to assure the required distillate production. This controller must be applied over the temperature instead of the water flow rate to include the following constraints:

$$1\,^{\circ}\mathrm{C} \leq T_{oF,ref} - T_{iF} \leq 20\,^{\circ}\mathrm{C} \tag{14}$$

$$T_h \leq T_{oF,ref} \leq 95\,^{\circ}\mathrm{C} \tag{15}$$

The solar-field outlet-inlet temperature difference must be lower than 20 °C to avoid stress in the absorber tubes; a minimum temperature difference must be guaranteed to avoid cooling down the water; T_{oF} must be under 95 °C to avoid evaporation, and it should be higher than T_h not to cool down the stored water.

Although most of the MPCs are applied to linear models, some techniques have been developed to obtain the future control actions using a nonlinear model of the process [25]. In this work, the Nonlinear Extended Prediction Self-Adaptive Control (NEPSAC) approach [26] has been chosen, because it directly uses the nonlinear prediction model without local linearization, and it solves the optimization problem in a low computational time. The idea behind this technique is to use the nonlinear model to predict the base and the step responses.

4.3. Regulatory Layer

The outlet solar-field temperature, T_{oF}, can be controlled by varying the solar-field water mass flow rate, $\dot{m}_F$, in its operating range [1, 3.2] kg/s. Several algorithms have been tested in this plant, obtaining successful results [19,27–31]. In this case, the feedback linearization control (FLC) is used [19]. A PI controller, with the valve γ_M as the control variable, is implemented to reach the desired T_{iM}.

5. Simulation Results

This section shows the results of the proposed control scheme under different meteorological conditions and with different curves of water volume demanded by the greenhouse. A comparison with the results obtained when no reference layer is included is also presented at the end of this section. With the aim of scaling the greenhouse water consumption to the solar desalination production, 10 greenhouses have been considered in the simulation. Therefore, the real consumption values obtained from the greenhouse have been multiplied by 10. The setpoint in the distillate tank has been established to 36 m^3 in order to store water for three days in case of cloudy days.

5.1. Sunny Day

In this example, the solar irradiance follows the Sun curve almost perfectly (Figure 7a). At the beginning, the stored water is equal to the setpoint (Figure 7d), and the temperatures in the cold and hot tanks are 72 °C and 76 °C, respectively (see Figure 7c). When irradiance reaches 500 W/m^2, the *PlantReady* signal is switched to one, and the MED unit is turned on (at 10:30 in Figure 7b; CM = 1), as well as the reference layer is activated. Since the estimated consumed water curve is under the real consumption (Figure 7g, blue and red lines, respectively), the inlet MED temperature setpoints, $T_{iM,ref}$, have lower values most of the time (between 55 °C and 60 °C, as can be observed in Figure 7h). The highest setpoint (68 °C at 11:00) is a consequence of the highest difference (3.7 m^3) between the distillate volume and the setpoint (V_d and $V_{d,ref}$ in Figure 7d). In the regulatory layer, the inlet MED temperatures are properly controlled with the valve aperture, which regulates the mass flow rate (Figure 7i).

To reach the desired temperatures at the inlet of the MED unit (Figure 7h, dashed line), the hot tank must also reach these temperatures, $T_{h,ref} = T_{iM,ref}$. However, in this case, T_h (Figure 7c, dashed line) is quite higher than $T_{iM,ref}$ (Figure 7e, dashed line), so the NMPC calculates that, with those irradiance conditions, the outlet temperature setpoint, $T_{oF,ref}$, must be the maximum one, so the water mass flow rate is close to the minimum one (Figure 7e), reducing the thermal energy delivered to the hot tank. As a consequence, the electricity consumption from the solar field pump is also reduced.

It is important to mention that, when the solar field is in recirculation mode (γ_t = 1 in Figure 7b), the NMPC output is different. In those situations, the calculated setpoints ($T_{oF,ref}$ in Figure 7e) are close to the minimum allowed to extend the recirculation mode period and reduce the temperature in the tanks. Although these situations happen in small periods of time (usually at startup and shut-down), this is a non-desirable consequence that should be avoided.

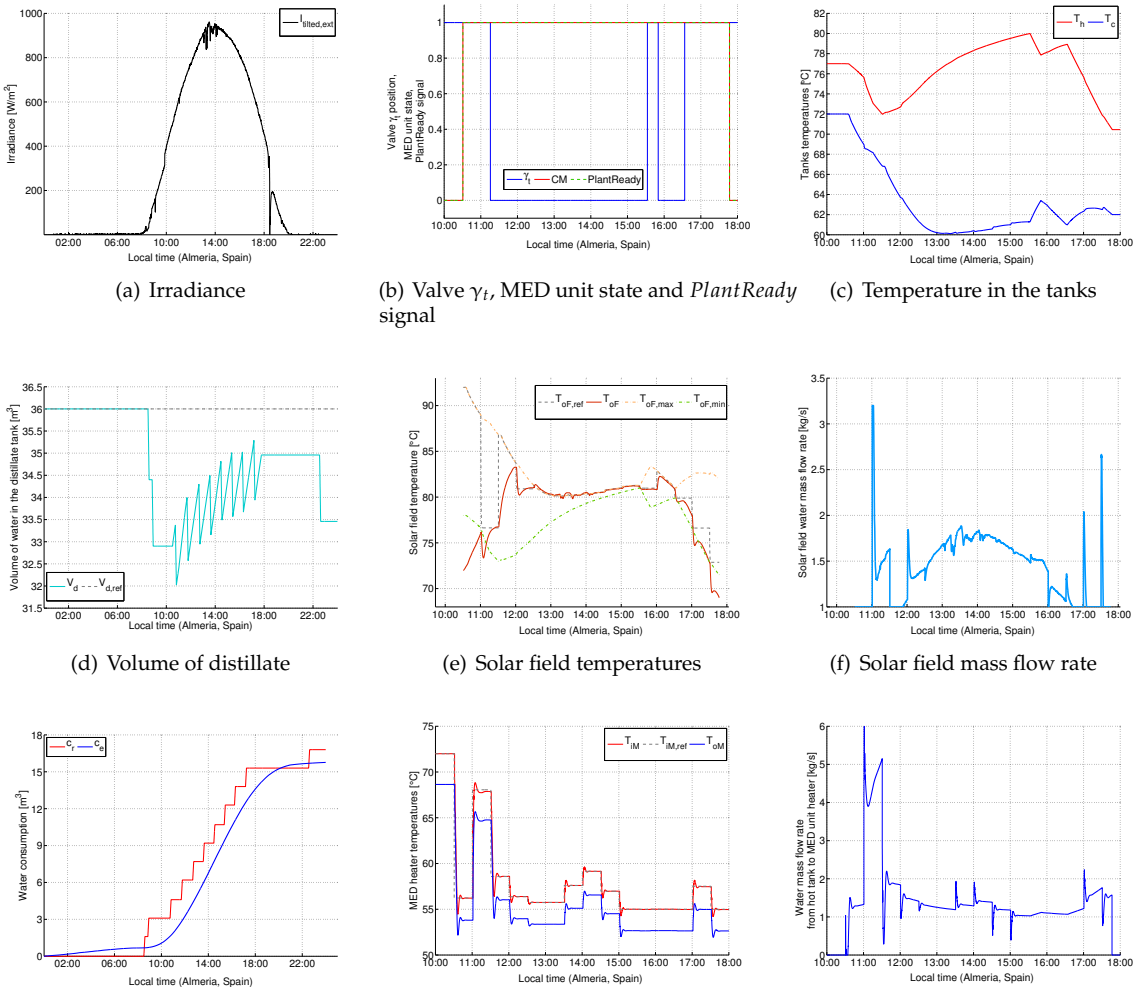

(a) Irradiance

(b) Valve γ_t, MED unit state and *PlantReady* signal

(c) Temperature in the tanks

(d) Volume of distillate

(e) Solar field temperatures

(f) Solar field mass flow rate

(g) 800-m^2 greenhouse water consumption

(h) Heater temperatures

(i) Heater mass flow rate

Figure 7. Simulation results obtained for a sunny day. (**a**) Irradiance; (**b**) Valve γ_t, MED unit state and *PlantReady*; (**c**) Temperature in the tanks; (**d**) Volume of distillate; (**e**) Solar field temperatures; (**f**) Solar field mass flow rate; (**g**) 800-m^2 greenhouse water consumption; (**h**) Heater temperatures; (**i**) Heater mass flow rate;

5.2. Partly Cloudy Day

In this example, the irradiance curve shows low fluctuations due to light clouds (Figure 8a), and the water consumption slightly overestimates the real demand (Figure 8g).

At the beginning, when the MED unit is started at 10:30 (Figure 8b, red line), the volume of distillate water is lower than the desired one (Figure 8g), so the inlet MED temperature setpoint is 69 °C (Figure 8h, dashed line) to compensate the estimated consumption. Due to the low temperature in the hot tank (Figure 8b, red line), this MED temperature is not feasible. The mass flow rate from the hot tank to the MED unit is the maximum one producing a quick stored thermal energy reduction (T_h falls down 9 °C in 1 h, as can be observed in Figure 8c). At 11:30, the stored distillate volume, V_d, is higher than the one desired, $V_{d,ref}$ (Figure 8d), and the inlet MED temperature setpoint (Figure 8h, dashed line) falls down to the minimum value (55 °C). As can be observed, this temperature, which assures low water production, is maintained during six hours. Nevertheless, the water production exceeds by 4 m^3 the one demanded, highlighting the challenge of coupling the production-demand variabilities.

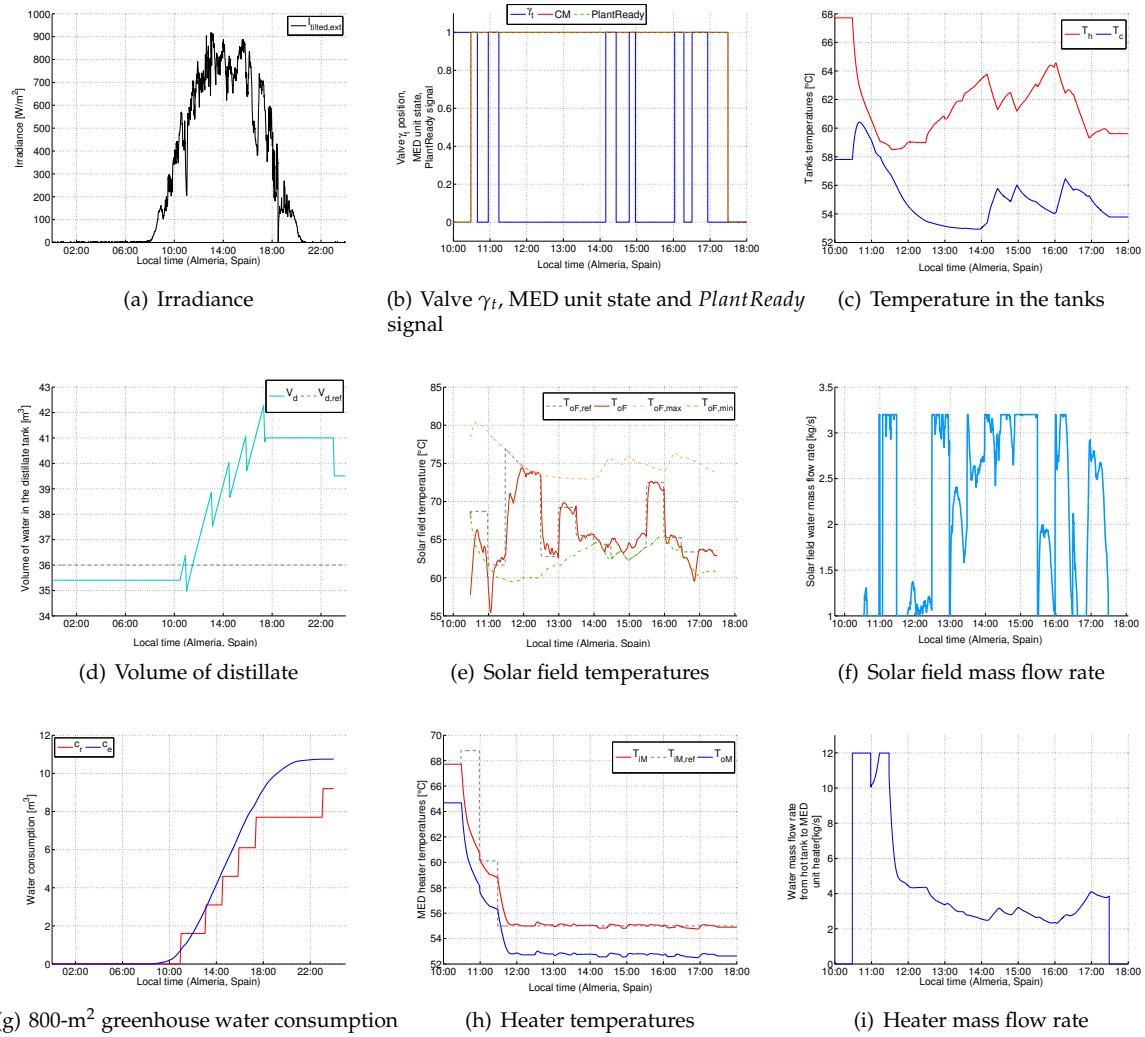

(a) Irradiance (b) Valve γ_t, MED unit state and *PlantReady* signal (c) Temperature in the tanks

(d) Volume of distillate (e) Solar field temperatures (f) Solar field mass flow rate

(g) 800-m^2 greenhouse water consumption (h) Heater temperatures (i) Heater mass flow rate

Figure 8. Simulation results obtained for a partly cloudy day. (**a**) Irradiance; (**b**) Valve γ_t, MED unit state and *PlantReady*; (**c**) Temperature in the tanks; (**d**) Volume of distillate; (**e**) Solar field temperatures; (**f**) Solar field mass flow rate; (**g**) 800-m^2 greenhouse water consumption; (**h**) Heater temperatures; (**i**) Heater mass flow rate;

In order to maintain the temperature in the hot tank close to $T_{iM,ref}$, the reference layer must change the solar field temperature setpoint (Figure 8e, dashed line), depending on the irradiance level, the solar field mode and the tanks temperatures. In this case, the solar field water mass flow rate (Figure 8e) shows more variation due to the irradiance disturbances. This example also shows a second situation that must be avoided. When the temperature in the hot tank is too much higher than the one desired in the MED unit, the mass flow rate from the hot tank to the MED unit can be higher than the solar field water mass flow rate, and part of the water flows from the hot to the cold tank (inverted flow situation). Under these conditions, the NMPC output gives lower solar field temperature setpoints to increase the solar field water mass flow rate, increase the quantity of water that flows from the hot to the cold tank and reduce the hot tank temperature more quickly. Although this fact happens in very reduced moments, obviously, this situation is undesirable, because stored thermal energy is being lost, and the electrical energy consumption from the solar field pump is being increased.

5.3. Ten Days

The proposed control strategy has been simulated during 10 days using greenhouse irradiance data measured in April 2015 (see Figure 9a). As Figure 9a shows, during the first five days, the distillate volume is maintained around the setpoint, with the higher deviation (Day 3) caused, in part, by a water consumption overestimation. During the following four days, the low solar irradiance level causes a severe fall in the distillate volume, and two weeks with good solar irradiance will be required to recover the desired level. This situation reveals the necessity of considering an auxiliary system to feed the MED unit or to have a backup of water from the district network if available. It must be pointed out that on the seventh day, the MED unit is not operated due to the low irradiance level. On the 10th day, the clouds disappear; the solar distillate plant can be operated again during almost six hours, and the volume of distillate starts its recovery.

Figure 9 shows the water and the solar field electrical energy consumptions. The mean error between the real and simulated water consumption is 0.07 m^3, and the maximum deviation is 0.16 m^3 on the third day. The electrical energy consumption depends on the irradiance level, volume of distillate and the MED unit operating hours; on sunny days in which the volume of distillate is close to the setpoint, such as the first day, the MPC provides low inlet MED temperature setpoints to reduce the water production. Therefore, lower tank temperatures are required, and the NMPC gives high solar field temperature setpoints, because it requires lower mass flow rates, which means a thermal energy reduction. For this reason, the electrical energy related to the pump is low. Nevertheless, if the distillate level is far from the setpoint and the water consumption estimation is high, the controller tries to increase the thermal energy from the solar field, and the electrical energy increases (see the second day). On the third day, the situation could be similar to the first day, but the electrical energy increases due to the undesirable situation (inverted flow) explained in Section 5.2. When the irradiance level is low, the electrical energy is also reduced, because the operating time is considerably lower, and the mass flow rate must be around the minimum value. In days, such as the 10th one (good irradiance level, but poor quantity of stored distillate), the system requires high solar field mass flow rates to increase the thermal energy and the water production, causing also an increment in the electrical energy consumption.

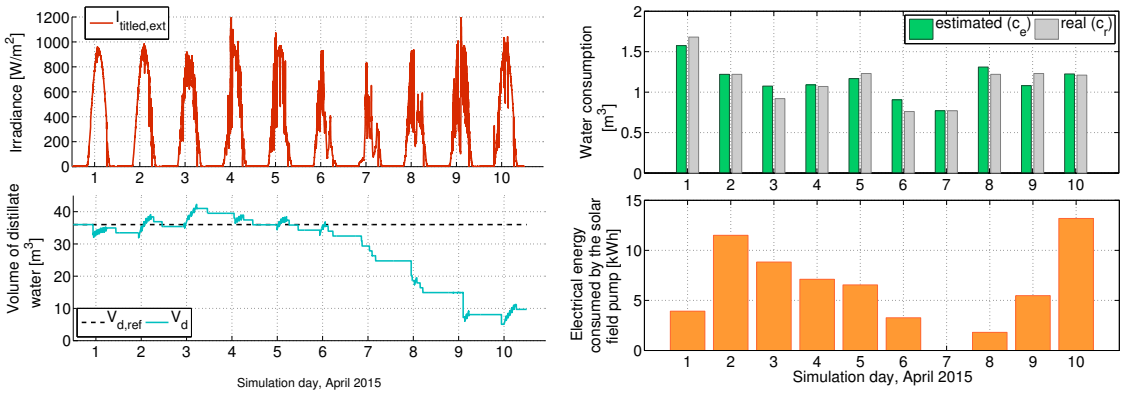

(a) Irradiance and distillate volume

(b) 800-m^2 greenhouse water consumption and solar field electrical energy consumption

Figure 9. Simulation results obtained during ten days. (**a**) Irradiance and distillate volume; (**a**) 800-m^2 greenhouse water consumption and solar field electrical energy consumption

5.4. Results without the Reference Layer

In order to observe the benefits of using the reference layer, the previous results have been compared to a case without a reference layer (see Table 2). In these simulations, it is considered $T_{iM,ref} = T_{oF,ref}$ =72 °C. The advantages are: lower electrical energy consumed in the solar field, P_F, higher energy storage in the tanks, E_a, and a lower integral of the absolute error (IAE), which is a performance index defined as $\int |V_{d,ref} - V_d| dt$. The disadvantage is that the MED unit must be operated more hours, increasing then the electrical energy consumed in the plant.

Table 2. Results for Days 1–10.

Reference Layer	IAE(m^3)	P_F (kWh)	E_a (GJ)	MED Operating Hours
Yes	7.3524×10^6	61.7	24.018	42.5
No	7.7793×10^6	64.4	23.985	38.5

6. Conclusions

The use of an appropriate control scheme in a solar desalination plant for greenhouse irrigation purposes could assure the water demand, reduce electricity costs in the solar field pump and maintain more thermal energy in the storage system. Trying to reduce the cost of the water produced in a solar desalination plant, a hierarchical controller has been proposed to maintain a distillate volume for greenhouse irrigation. Promising results have been obtained from the fact that dynamic models of both demand and production systems can be the key for reaching more competitive distillate prices when model predictive controllers are applied. Nevertheless, some remarks have to be highlighted to improve the results: (i) the control objective should be changed to minimize the distillate cost taking into account distillate volume constraints; (ii) an external source of energy could be included to assure a continuous production of water (when a water backup is not available); (iii) simulation in different seasons should be included to consider the variability in the crop state and in the hydric requirements.

Acknowledgments: This work has been funded by the National Plan Project DPI2014-56364-C2-1-R of the Spanish Ministry of Economy and Competitiveness and ERDF funds and by the Controlcrop Project, P10-TEP-6174, project framework, supported by the Andalusian Ministry of Economy, Innovation and Science (Andalusia, Spain).

Author Contributions: Lidia Roca has carried out most of the work presented in this paper. Jorge A. Sánchez and Francisco Rodríguez have contributed with the greenhouse knowledge; they have shared the greenhouse model and experimental data. Javier Bonilla and Alberto de la Calle have contributed with the MED unit model, and Manuel Berenguel has contributed to the control strategy. All of the authors have participated in the manuscript revision.

Conflicts of Interest: The authors declare no conflict of interest.

Nomenclature

Symbol	Description	Units
A	Area	(m^2)
c	Water consumption	(m^3)
c_p	Specific thermal capacity	(J/kg°C)
d	Discharge coefficient	(-)
DPV	Vapour pressure deficit	(Pa)
g	Gravitational acceleration	(m/s^2)
h	Heat transfer coefficient	(W/m^2°C)
H	Absolute humidity	(kg water/kg air)
I	Irradiance	(W/m^2)
k_l	Light extinction coefficient	(-)
k_w	Wind-effect coefficient	(-)
l	Length	(m)
LAI	Leaf area index	(m^2 leaves/m^2 soil surface)
$\dot{m}$	Mass flow rate	(kg/s)
$\dot{M}$	Mass flow rate per square meter	(kg/s m^2)
n	Number of vents	(-)
q	Volumetric flow	(m^3/s)
Q	Heat flux	(W/m^2)
t	Time	(s)
t_s	Sampling time	(s)
T	Temperature	(°C)
U	Vent position	(%)
v_w	Wind speed	(m/s)
V	Volume	(m^3)
w	Width of vent	(m)
λ	Vaporization air latent heat	(J/kg)
ρ	Density	(kg/m^3)
γ	Valve position	(-)

Subscript	Description
a	Air
amb	Ambient
c	Cold tank
cd	Condensation
cnv	Convective
$cord$	Ventilation cord
cr	Crop
cv	Cover
d	Distillate
e	Estimation
exh	Exhaust
ext	Exterior
evp	Evaporation
F	Solar field
g	Greenhouse
h	Hot tank
i	Inlet
int	Interior
lim	Limit
$loss$	Leakage
max	Maximum
min	Minimum
M	MED
o	Outlet
r	Real
ref	Setpoint
ss	Soil surface
t	Tank
trp	Transpiration
ven	Ventilation

References

1. Sánchez-Martos, F.; Pulido, A.; Calaforra, J.M. Hydrogeochemical processes in an arid region of Europe (Almeria, SE Spain). *Appl. Geochem.* **1999**, *14*, 735–745.
2. Fernández, M.D.; González, A.M.; Carreño, J.; Pérez, C.; Bonachela, S. Analysis of on-farm irrigation performance in Mediterranean greenhouses. *Agric. Water Manag.* **2007**, *89*, 251–260.
3. Li, C.; Goswami, Y.; Stefanakos, E. Solar assisted sea water desalination: A review. *Renew. Sustain. Energy Rev.* **2013**, *19*, 136–163.
4. Chaibi, M.T. An overview of solar desalination for domestic and agriculture water needs in remote arid areas. *Desalination* **2000**, *127*, 119–133.
5. Hosseini, S.R.; Amidpour, M.; Shakib, S.E. Cost optimization of a combined power and water desalination plant with exergetic, environment and reliability consideration. *Desalination* **2012**, *285*, 123–130.
6. Salcedo, R.; Antipova, E.; Boer, D.; Jiménez, L.; Guillén-Gosálbez, G. Multi-objective optimization of solar Rankine cycles coupled with reverse osmosis desalination considering economic and life cycle environmental concerns. *Desalination* **2012**, *286*, 358–371.
7. Shakib, S.E.; Hosseini, S.R.; Amidpour, M.; Aghanajafi, C. Multi-objective optimization of a cogeneration plant for supplying given amount of power and fresh water. *Desalination* **2012**, *286*, 225–234.
8. Wu, L.; Hu, Y.; Gao, C. Optimum design of cogeneration for power and desalination to satisfy the demand of water and power. *Desalination* **2013**, *324*, 111–117.
9. Alarcon-Padilla, D.; Blanco-Gálvez, J.; García-Rodríguez, L.; Gernjak, W.; Malato, S. First experimental results of a new hybrid solar/gas multi-effect distillation system: The AQUASOL project. *Desalination* **2008**, *220*, 619–625.
10. Palenzuela, P.; Alarcón, D.; Blanco, J.; Guillén, E.; Ibarra, M.; Zaragoza, G. Modeling of the heat transfer of a solar multi-effect distillation plant at the Plataforma Solar de Almería. *Desalination Water Treat.* **2011**, *31*, 257–268.
11. Rodríguez, F.; Berenguel, M.; Guzmán, J.; Ramírez-Arias, A. *Modeling and Control of Greenhouse Crop Growth*; Springer: Cham, Switzerland, 2015; p. 250.
12. Chalabi, Z.; Bailey, B. *Simulation of the Energy Balance in a Greenhouse. Divisional Note, 1516*; Technical report, Silsoe Research Institute: Silsoe, Bedford, UK, 1989.
13. Wan-Liang, W.; Qi-Di, W. Neural network modelling and intelligence control of the distributed parameter greenhouse climate. In Proceedings of the 14th IFAC World Congress, Beijing, China, 5–9 July 1999; Volume 1, pp. 479–484.
14. ASAE. *Heating, Ventilating, and Cooling Greenhouses (EP406.3)*; American Society of Agricultural Engineering Standards: St. Joseph, MI, USA, 1998.
15. Berenguel, M.; Rodríguez, F.; Guzmán, J.; Lacasa, D.; Pérez-Parra, J. Greenhouse diurnal temperature control with natural ventilation based on empirical models. *Acta Hortic.* **2006**, *719*, 57–64.
16. Seginer, I. Some artificial neural network applications to greenhouse environmental control. *Comput. Electron. Agric.* **1997**, *18*, 167–186.
17. Sánchez-Molina, J.; Rodríguez, F.; Guzmán, J.L.; Arahal, M. Virtual sensors for designing irrigation controllers in greenhouses. *Sensors* **2012**, *11*, 15244–15266.
18. Baille, M.; Baille, L.; Laury, J.C. A simplified model for predicting evapotranspiration rate of nine ornamental species vs. climate factors and leaf area. *Sci. Hort.* **1994**, *59*, 217–232.
19. Roca, L.; Berenguel, M.; Yebra, L.; Alarcón-Padilla, D. Solar field control for desalination plants. *Sol. Energy* **2008**, *82*, 772–786.
20. Roca, L.; Yebra, L.J.; Berenguel, M.; Alarcon-Padilla, D. Modeling of a Solar Seawater Desalination Plant for Automatic Operation Purposes. *J. Sol. Energy. Eng.* **2008**, *130*, 041009:1–041009:8.
21. de la Calle, A.; Bonilla, J.; Roca, L.; Palenzuela, P. Dynamic modeling and simulation of a solar-assisted multi-effect distillation plant. *Desalination* **2015**, *357*, 65–76.
22. Åström, K.J.; Hägglund, T. *PID Controllers: Theory, Design, and Tunning*; Instrument Society of America; Durham, NC, USA, 1995.
23. Franklin, G.F.; Powell, J.D.; Emami-Naeini, A. *Feedback Control of Dynamic Systems*; Prentice Hall: Upper Saddle River, NJ, USA, 2010.

24. Duffie, J.A.; Beckman, W.A. *Solar Engineering of Thermal Processes*, 4th ed.; Joh Wiley & Sons: Hoboken, NJ, USA, 2013; p. 936.
25. Camacho, E.F.; Bordons, C. *Model Predictive Control*; Springer: London, UK, 2013.
26. De Keyser, R. Model based predictive control for linear systems. In *UNESCO Encyclopaedia of Life Support Systems (EoLSS);* Eolss Publishers Co Ltd: Oxford, UK, 2003.
27. Ayala, C.O.; Roca, L.; Guzman, J.L.; Normey-Rico, J.E.; Berenguel, M.; Yebra, L.J. Local model predictive controller in a solar desalination plant collector field. *Renew. Energ.* **2011**, *36*, 3001–3012.
28. Roca, L.; Guzman, J.L.; Normey-Rico, J.E.; Berenguel, M.; Yebra, L.J. Robust constrained predictive feedback linearization controller in a solar desalination plant collector field. *Control. Eng. Pract.* **2009**, *17*, 1076–1088.
29. Roca, L.; Guzman, J.L.; Normey-Rico, J.E.; Berenguel, M.; Yebra, L.J. Filtered Smith predictor with feedback linearization and constraints handling applied to a solar collector field. *Sol. Energy* **2011**, *85*, 1056–1067.
30. Torrico, B.C.; Roca, L.; Normey-Rico, J.E.; Guzman, J.L.; Yebra, L.J. Robust Nonlinear Predictive Control Applied to a Solar Collector Field in a Solar Desalination Plant. *IEEE. Trans. Control Syst. Technol.* **2010**, *18*, 1430–1439.
31. Santos, T.; Roca, L.; Guzman, J.L. Practical MPC with robust dead-time compensation applied to a solar desalination plant. In Proceedings of the 18th IFAC World Congress, Milano, Italy, 28 August–2 September 2011; pp. 4909–4914.